Virologica Sinica 40 (2025) 755–768

Contents lists available at ScienceDirect

Virologica Sinica

journal homepage: www.keaipublishing.com/en/journals/virologica-sinica
www.virosin.org

Research Article

SNX10 enhances HCoV-OC43 infection by facilitating viral entry and inhibiting virus-triggered autophagy

Haobin Li [a], Huiyi Guo [a], Binhao Rong [a], Haowei Li [a], Wenjiao Wu [b], Chan Yang [a,c], Shuwen Liu [a,c,d,e,*]

[a] Guangdong-Hongkong-Macao Joint Laboratory for New Drug Screening, Guangdong Provincial Key Laboratory of New Drug Screening, School of Pharmaceutical Sciences, Southern Medical University, Guangzhou, 510515, China
[b] Department of Pharmacy, Jinan University Affiliated Guangdong Second Provincial General Hospital, Guangzhou, 510317, China
[c] MOE Key Laboratory of Infectious Diseases Research in South China, MOE Innovation Center for Medical Basic Research on Inflammation and Immune Related Diseases, Southern Medical University, Guangzhou, 510515, China
[d] NMPA Key Laboratory for Research and Evaluation of Drug Metabolism, Department of Pharmacy, Pingshan Hospital, Southern Medical University, Shenzhen, 518100, China
[e] State Key Laboratory of Organ Failure Research, Guangdong Provincial Institute of Nephrology, Southern Medical University, Guangzhou, 510515, China

ARTICLE INFO

Keywords:
Sorting nexin 10 (SNX10)
Coronavirus infection
Host factor
Endosomal acidification
Autophagic flux

ABSTRACT

The ongoing coronavirus epidemic, including the novel coronavirus (SARS-CoV-2), continues to pose a significant threat to global public health. Host targets address multiple stages of the viral life cycle and provide diverse opportunities for therapeutic interventions. This study identified sorting nexin 10 (SNX10) as a facilitator of replication of human coronavirus OC43 (HCoV-OC43), underscoring its potential as a novel antiviral target. The knockout of *SNX10* significantly suppressed HCoV-OC43 replication both *in vivo* and *in vitro*. Immunoprecipitation-mass spectrometry (IP-MS) analysis identified the adaptor protein complex 2 subunit μ1 (AP2M1) as a direct interactor of SNX10. Specifically, SNX10 facilitates phosphorylation of the AP2M1, thereby enhancing clathrin-mediated viral endocytosis. Furthermore, subsequent binding and internalization assays revealed that *SNX10* knockout significantly inhibits viral entry into host cells. Conversely, the reconstitution of SNX10 fully restored viral entry, thereby confirming the critical and indispensable role of SNX10 in pathogen internalization. Simultaneously, SNX10 was identified as a key factor that promotes endosomal acidification by modulating pH levels, which in turn facilitated the release of the viral genome. Notably, the ablation of SNX10 was found to trigger autophagy activation during infection, thereby maintaining intracellular homeostasis. Additionally, it exerted autonomous antiviral effects through lysosomal degradation pathways. Collectively, these findings demonstrate SNX10 serves as a pivotal regulator of the viral life cycle and underscore its therapeutic potential as a multi-faceted antiviral candidate target capable of simultaneously inhibiting viral internalization, viral genomic release, and host-pathogen equilibrium.

INTRODUCTION

Human coronavirus OC43 (HCoV-OC43) was first identified as a betacoronavirus in 1967. It is an enveloped virus with a single-stranded positive-strand RNA genome (Kesheh et al., 2022). The most commonly reported symptoms in HCoV-OC43 infected individuals include sore throat, cough, and rhinorrhea. Additionally, the virus has been shown to possess neuroinvasive properties. As one of the seven coronaviruses capable of infecting humans, HCoV-OC43 is classified within the *Coronaviridae* family and belongs to the *Betacoronavirus* genus (Vijgen et al., 2005). HCoV-OC43 contains four structural proteins: the spike (S) protein, envelope E) protein, membrane (M) protein and nucleocapsid (N)

* Corresponding author.
E-mail address: liusw@smu.edu.cn (S. Liu).

https://doi.org/10.1016/j.virs.2025.07.005
Received 22 March 2025; Accepted 7 July 2025
Available online 9 July 2025
1995-820X/© 2025 The Authors. Publishing services by Elsevier B.V. on behalf of KeAi Communications Co. Ltd. This is an open access article under the CC BY-NC-ND license (http://creativecommons.org/licenses/by-nc-nd/4.0/).

protein (Schmidt et al., 2017). Among these, the S protein facilitates host attachment and mediates the fusion of the virus with the cell membrane during viral infection by binding to the receptor 9-O-acetylsalivaryl acid (9-O-Ac-Sia) (Wang et al., 2022), subsequently entering the cell *via* the endocytosis pathway. Viral genomic RNA (gRNAs) serve as templates for the translation of polyproteins (pp1a and pp1ab), which are subsequently cleaved to generate viral non-structural proteins (NSPs) (Malik, 2020; Peng et al., 2020). NSPs induce the rearrangement of the cell membrane, leading to the formation of double-membrane vesicles (DMVs) in which viral replication transcriptional complexes (RTCs) are anchored (Chen et al., 2020). Full-length gRNAs are replicated *via* negative-strand intermediates, and a nested set of gRNAs is synthesized through discontinuous transcription (Malone et al., 2022). These gRNAs encode viral structural components and accessory proteins (Tan et al., 2006). The resultant viral product is assembled within the endoplasmic reticulum-Golgi intermediate complex and subsequently buds onto the plasma membrane in the form of smooth-walled vesicles that are expelled from the cell *via* exocytosis (Brian and Baric, 2005; Fehr and Perlman, 2015).

Binding to the receptor initiates the process. The binding may induce direct fusion of the virus with the cell membrane; however, in most instances, the virus is internalized *via* the endocytosis pathway and subsequently encapsulated within smooth-walled vesicles (Hussain et al., 2011). One of the most common endocytosis pathways is clathrin protein-mediated endocytosis, and a variety of viruses are internalized *via* this endocytosis pathway. Upon recognition by the receptor, the viral particle docks into the clathrin-protein-mediated pit, recruits articulin protein 2 (AP2) to the nucleation site *via* Epsin1 (Henne et al., 2010) to form the vesicle's outgrowth structure. This structure is subsequently engaged to supply energy to kinesin, ultimately leading to the detachment of the vesicle from the cell surface and the formation of a cargo-containing vesicle (Cocucci et al., 2014).

SNX10 is a member of the sorting nexins (SNXs) family, which is involved in endosomal sorting processes. All members possess a phox (PX) domain (Liao et al., 2024), which serves as a phosphoinositide-binding module that facilitates the formation of endosomal transport carriers through either reverse-transcription-dependent or independent mechanisms (Schmidt et al., 2017; Amatya et al., 2021). The proteins in SNXs family play various roles in cargo sorting, retrograde protein transport, and lysosomal degradation (Lu et al., 2022). Compared with other SNXs family members, SNX10 has a relatively simple structure and does not contain any other known functional structural domains, except for the PX structural domain (Van Weering et al., 2010; Norris et al., 2017; Tian et al., 2021). In this study, we focused on the regulation of SNX10 during HCoV-OC43 infection.

Current research demonstrates that SNX10 plays a critical role in cilia formation. Knockdown of *SNX10* suppresses cilia formation by depending on V-ATPase activity, and the acidic pH environment of endosomes activates cathepsin L (Tscherne et al., 2006), triggering the fusion of the viral envelope with the membrane of the endosomes thereby releasing the viral genome. Knockdown of *SNX10* inhibits the activity of cathepsin A (Wang et al., 2021), enhances the stability of lysosome-associated membrane protein-2A (LAMP-2A), and activates chaperone-mediated autophagy (You et al., 2018). However, some viruses can facilitate their replication by actively modulating or channelizing autophagy. For instance, dengue virus utilizes autophagosomal membranes as scaffolds for its replication complexes (Yousefi et al., 2022). Upon viral infection, selective autophagy receptors typically recognize viral components, thereby initiating 'xenophagy' (Kong et al., 2020), enhancing autophagy levels, and inhibiting viral proliferation, which collectively safeguards cells from pathogen-induced damage (Miller et al., 2020).

In this study, we aimed to elucidate the role of SNX10 as a host factor that facilitates viral infection and tried to provide valuable insights for future responses to coronavirus outbreaks. Furthermore, we will investigate the potential of targeting SNX10 for the development of therapeutic agents.

RESULTS

SNX10 deletion inhibits viral replication *in vivo*

To investigate the role of SNX10 in viral pathogenesis, we generated conditional *Snx10* knockout (CKO) mice with lung epithelial cell-specific deletions as the experimental group and compared them with wild-type (WT) mice serving as the control group. Using HCoV-OC43 infection to establish a murine pneumonia model, we observed that while the virus did not cause severe pulmonary damage, WT mice exhibited more pronounced lung inflammation compared to CKO mice. Immunohistochemical analysis demonstrated significantly elevated expression of the viral nucleocapsid (NP) protein in the lung tissue of the WT group (Fig. 1A, B). Histopathological examination revealed characteristic alveolar interstitial thickening, tissue edema, increased mucus secretion, and prominent inflammatory cell infiltration in the infected lungs. Notably, CKO mice demonstrated markedly reduced pulmonary inflammation and significantly lower pathological scores compared to WT mice (Fig. 1C, D). Although no significant intergroup differences were detected in lung indices or inflammatory cytokine levels (Fig. 1E–I), quantitative analysis revealed markedly decreased NP protein levels in CKO lung tissues (Fig. 1J and K). These findings suggest that *SNX10* deficiency compromises HCoV-OC43 viral replication *in vivo*.

SNX10 deficiency impairs viral replication *in vitro* and enhances protein stability

In vitro, we employed HCT-8 cells as a model to examine the replication dynamics of HCoV-OC43 virus at both the protein and transcriptional levels. CRISPR/Cas9-mediated *SNX10*-knockout cell line was successfully established (Fig. 2A). Subsequent *in vitro* infection assays demonstrated markedly impaired viral replication in *SNX10*-deficient cells compared with that in wild-type controls (Fig. 2B–D). Quantitative analysis revealed that HCoV-OC43 infection significantly upregulated SNX10 protein expression (Fig. 2E and F), while its mRNA levels remained unchanged (Fig. 2G). To elucidate the mechanism underlying SNX10 protein accumulation, we conducted cycloheximide (CHX) chase experiments. These experiments revealed showed enhanced protein stability in virus-infected cells, as evidenced by significantly slower degradation rates of SNX10 in the infected group compared to uninfected controls (Fig. 2H).

SNX10 interacts with the C-terminus of AP2M1 during viral infection

To investigate the molecular mechanism of SNX10 in viral entry, we established a stable HCT-8 cell line overexpressing SNX10 (Fig. 3A). Immunoprecipitation (IP) followed by silver staining identified distinct protein bands within the molecular weight range of 45–65 kDa in SNX10 complexes (Fig. 3B). Based on iBAQ quantification and functional correlation analysis, in conjunction with the silver staining results, AP2M1 was identified as the major interacting factor (Fig. 3C and D) (Helbig et al., 2019). Reciprocal co-IP assays in 293T cells validated the interaction between SNX10-AP2M1 (Fig. 3E and F). Additionally, immunofluorescence experiments confirmed that SNX10 co-localizes with AP2M1 (Fig. 3G). Domain mapping revealed that SNX10 specifically interacts with the C-terminal D2 domain of AP2M1 (AP2M1-C; Fig. 3H and I). Molecular docking simulations using ZDOCK predicted a high-affinity interaction (Z-score >4.5) between SNX10 and AP2M1-C

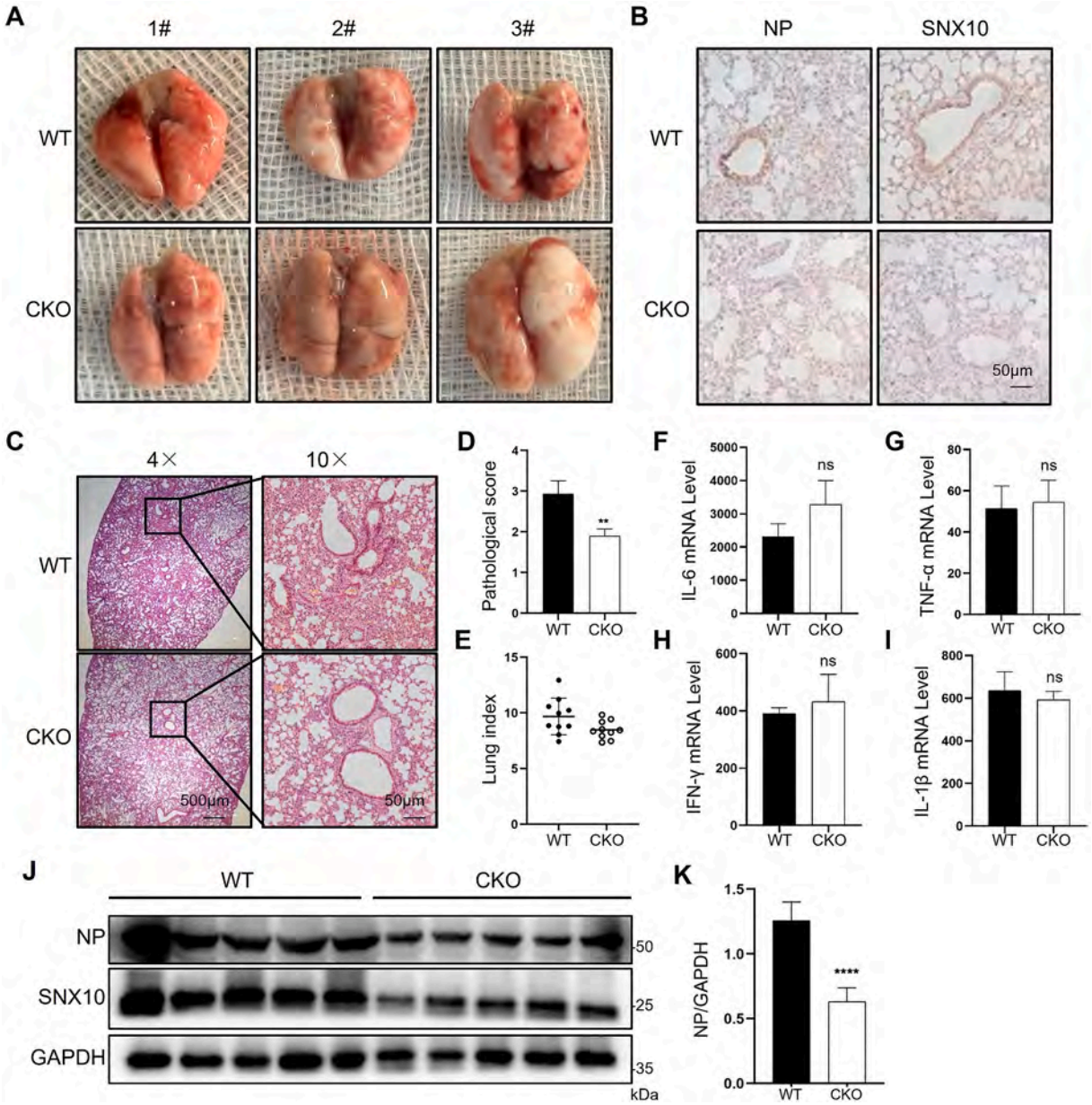

Fig. 1. The deletion of *SNX10* has been demonstrated to inhibit viral replication *in vivo*. Wild type C57BL/6J) (WT) and *Snx10* conditional knockout (CKO, *Snx10*$^{LEC-KO}$) mice (n = 10) were infected with HCoV-OC43 by nasal instillation (MOI = 10). Lung tissues were collected at day 3 post-infection (dpi). **A** Group comparison and lung histomorphology at 3 dpi. **B** Immunohistochemistry images of viral NP and SNX10 expression in lung tissue of WT and CKO mice at 3 dpi (Scale bar = 50 μm). **C–E** Hematoxylin and eosin images (**C**), pathological scores (**D**), and lung indices (**E**) of WT and CKO mice at 3 dpi (Scale bar = 50 μm). **F–I** RT-qPCR analysis of IL-6 (**F**), TNF-α (**G**), IFN-γ (**H**), and IL-1β (**I**) mRNA levels in lung tissue at 3 dpi. **J, K** Western blot analysis of viral NP and SNX10 expression (**J**) and NP/GAPDH ratios (**K**) in lung tissue at 3 dpi. The data are presented as the mean ± SEM, and *P* values were calculated using two-tailed Student's *t*-test. ** $P < 0.01$; **** $P < 0.0001$; ns, not significant, $P > 0.05$.

through complementary surface charge interactions (Fig. 3J and K). These findings provide a structural foundation for the functional partnership between SNX10 and AP2M1.

SNX10 deficiency impairs AP2M1 phosphorylation to restrict viral entry

We first confirmed that viral infection did not alter AP2M1 expression levels but markedly stimulated AP2M1 phosphorylation (Fig. 4A). Furthermore, AP2M1 is capable of forming a complex with clathrin proteins, and this modified complex facilitates cellular endocytosis. Further experimental results demonstrated that the deletion of SNX10 did not alter AP2M1 protein expression but significantly inhibited AP2M1 phosphorylation (Fig. 4B), which is critical for the stability and function of the complex. These findings suggest that *SNX10* deletion plays a pivotal role in suppressing the formation of the complex (Liu et al., 2021).

To investigate whether SNX10 mediates the interaction between AP2M1 and clathrin proteins, the MYC-AP2M1 vector was co-transfected with a series of HA-SNX10 expression vectors featuring incremental expression levels into 293T cells. The results demonstrated that the binding affinity between AP2M1 and clathrin progressively increased as the expression level of SNX10 was elevated (Fig. 4C). By fractionating the cytoplasmic proteins from the cell membrane, it was observed that SNX10 predominantly accumulated on the cell membrane, thereby facilitating the phosphorylation of AP2M1 (Fig. 4D).

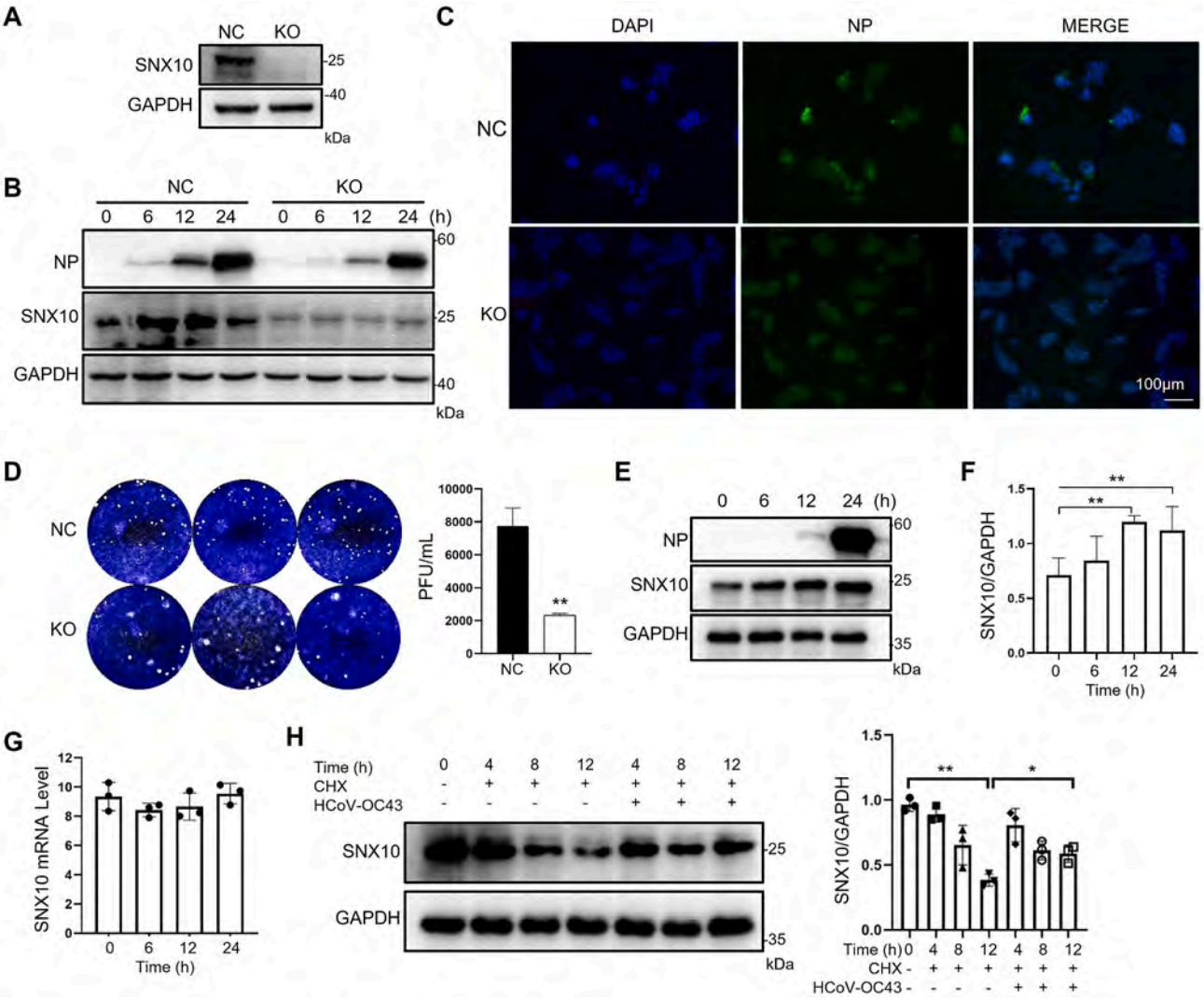

Fig. 2. *SNX10* deficiency affects viral replication *in vitro* and viral infection enhances SNX10 protein stability. **A** Western blot analysis of SNX10 protein expression in *SNX10*-knockout (KO) and control HCT-8 cells (NC). **B** Western blot analysis of viral NP and SNX10 expression in *SNX10*-KO and control HCT-8 cells with HCoV-OC43 infection (MOI = 1) at 24 hours post-infection (hpi). **C** Representative immunofluorescence images of viral NP expression in *SNX10*-KO and control HCT-8 cells with HCoV-OC43 infection (MOI = 1) at 24 hpi (Scale bar = 100 μm). **D** Plaque assay performed in RD cells to determine the viral titres collected from *SNX10*-KO and control HCT-8 cells infected with HCoV-OC43 (MOI = 1) at the 48 hpi. **E, F** Western blot analysis of viral NP and SNX10 expression in HCT-8 cells after HCoV-OC43 (MOI = 1) infection for 0, 6, 12 and 24 h. **G** RT-qPCR of SNX10 mRNA level in HCT-8 cells after HCoV-OC43 (MOI = 1) infection for 0, 6, 12 and 24 h. **H** Western blot analysis of SNX10 expression in HCT-8 cells treated with CHX (100 μg/mL) after HCoV-OC43 (MOI = 10) infection for 4, 8 and 12 h. Experiments were repeated three times. The data are presented as the mean ± SEM, and *P* values were calculated using two-tailed Student's *t*-test. * $P < 0.05$; ** $P < 0.01$.

After treatment of cells with DC-SX029 (an inhibitor of the SNX10 protein), it was demonstrated that DC-SX029 significantly suppressed viral replication. Additionally, when AAK1 (an inhibitor of AP2M1 phosphorylation) was employed as a positive control, AAK1 also effectively inhibited viral replication (Fig. 4E). We observed that SNX10 inhibition by DC-SX029 significantly suppressed AP2M1 phosphorylation, a finding consistent with the effects of the AAK1 (Fig. 4F). Immunofluorescence analysis further demonstrated that DC-SX029 treatment efficiently inhibited clathrin internalization while preserving normal clathrin expression levels (Fig. 4G).

Previous studies have demonstrated that SNX10 plays a pivotal role in endosomal acidification (Battaglino et al., 2019), a process that is essential for the entry of enveloped virus into cells. We hypothesized that SNX10 regulates the initial stage of viral entry during replication cycle. To verify whether SNX10 is involved in the entry phase of the HCoV-OC43 virus, we evaluated the regulatory role of SNX10 through a pseudoviral assay and discovered that deletion of *SNX10* significantly suppresses virus entry (Fig. 4H). We observed that SNX10 did not influence virus binding (Fig. 4I); however, the deletion of *SNX10* significantly impaired virus entry (Fig. 4J). Our results demonstrated that SNX10 primarily functions during the pre-viral entry stage in an acidic bypass assay (Fig. 4K). Furthermore, we employed the dyes DIO and DIL to specifically stain the viral membrane and cellular membrane, respectively, thereby enabling us to track the process of viral entry. This analysis revealed that the rate of viral entry was significantly reduced in the absence of SNX10 (Fig. 4L). These results suggest that deletion of SNX10 inhibits viral infection by blocking viral entry. It has been proposed that SNX10 directly interacts with AP2M1, thereby promoting the phosphorylation of AP2M1 and enhancing the interaction between AP2M1 and clathrin to facilitate viral entry.

SNX10 facilitates endosomal acidification

SNX10 knockout markedly inhibited viral replication. In contrast, the reconstitution of exogenous SNX10 in *SNX10* knockout (KO) cells not only restored viral entry efficiency but also significantly enhanced it

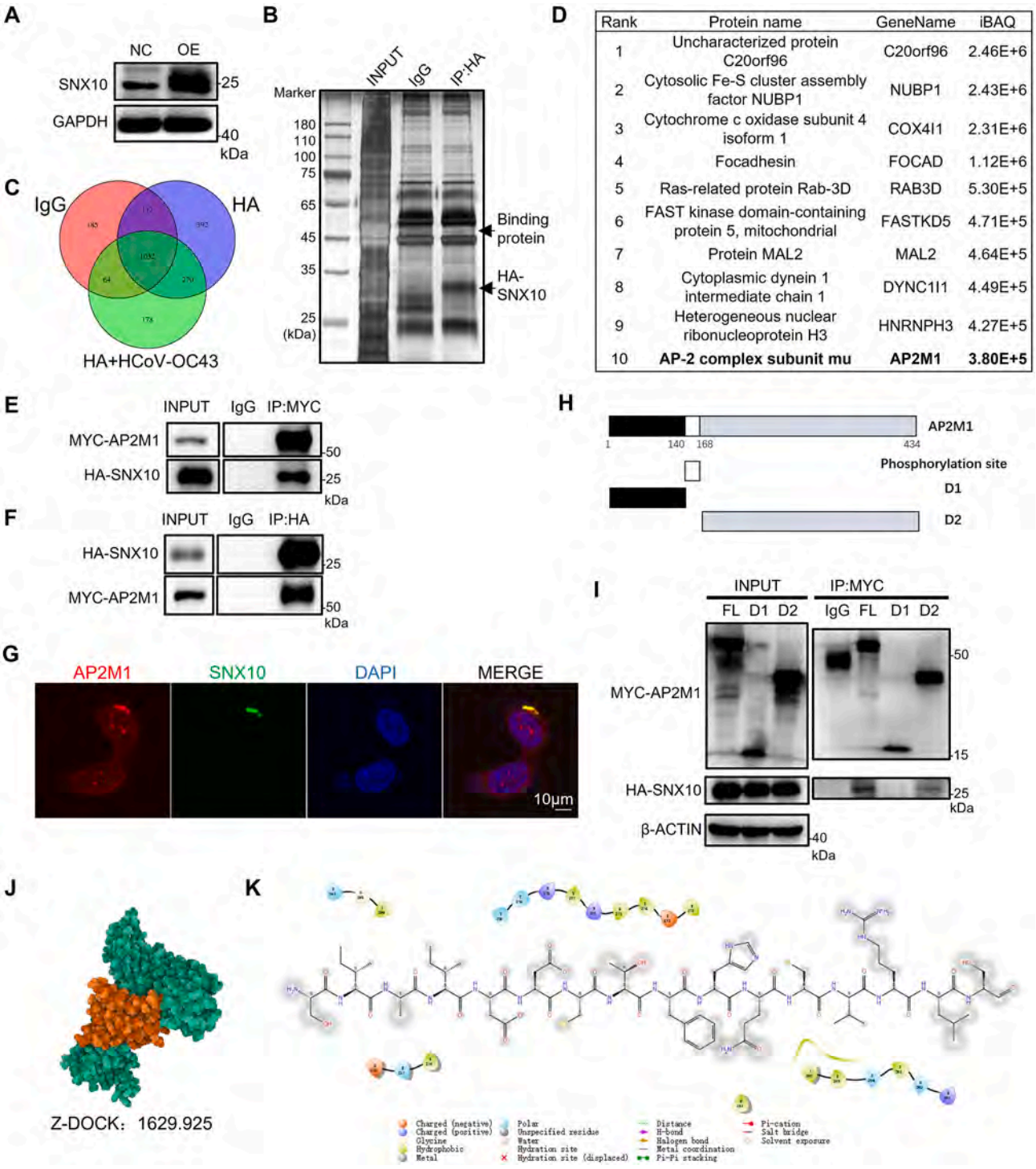

Rank	Protein name	GeneName	iBAQ
1	Uncharacterized protein C20orf96	C20orf96	2.46E+6
2	Cytosolic Fe-S cluster assembly factor NUBP1	NUBP1	2.43E+6
3	Cytochrome c oxidase subunit 4 isoform 1	COX4I1	2.31E+6
4	Focadhesin	FOCAD	1.12E+6
5	Ras-related protein Rab-3D	RAB3D	5.30E+5
6	FAST kinase domain-containing protein 5, mitochondrial	FASTKD5	4.71E+5
7	Protein MAL2	MAL2	4.64E+5
8	Cytoplasmic dynein 1 intermediate chain 1	DYNC1I1	4.49E+5
9	Heterogeneous nuclear ribonucleoprotein H3	HNRNPH3	4.27E+5
10	**AP-2 complex subunit mu**	**AP2M1**	**3.80E+5**

Fig. 3. AP2M1 directly interacts with SNX10 through cargo-binding domain recognition. **A** Western blot analysis of SNX10 expression in SNX10-HA overexpressing HCT-8 cells. **B** Silver staining of SDS-PAGE gels showed that the immunoprecipitates were pulled down by HA-Tag antibody from SNX10-HA overexpressing HCT-8 cells. The different bands of interest are indicated by black arrows. **C** Venn diagram for the intersection of immunoprecipitates were pulled down by IgG (red), HA-Tag antibody from HCoV-OC43 infection group (green) and HA-Tag antibody from control group (blue) to screen out the potential proteins directly interact with SNX10. **D** Based on the ranking of iBAQ scores of mass spectrometry results, we screened out the top 10 mutual support proteins with the highest probability. **E, F** Co-immunoprecipitation (Co-IP) for the interaction between SNX10 and AP2M1 in 293T cells. **G** Immunofluorescence images of colocalization of SNX10 and AP2M1 in HCT-8 cells after infection with HCoV-OC43. **H** The schematic of deletion truncations of MYC-AP2M1 overexpressing plasmids. **I** Co-IP for the interaction between different truncations of AP2M1 and SNX10 in 293T cells. **J, K** The schematic of docking between SNX10 to the C-terminal of AP2M1 (https://www.home-for-researchers.com/#/) and speculate on the location of the union of the two. Experiments were repeated three times.

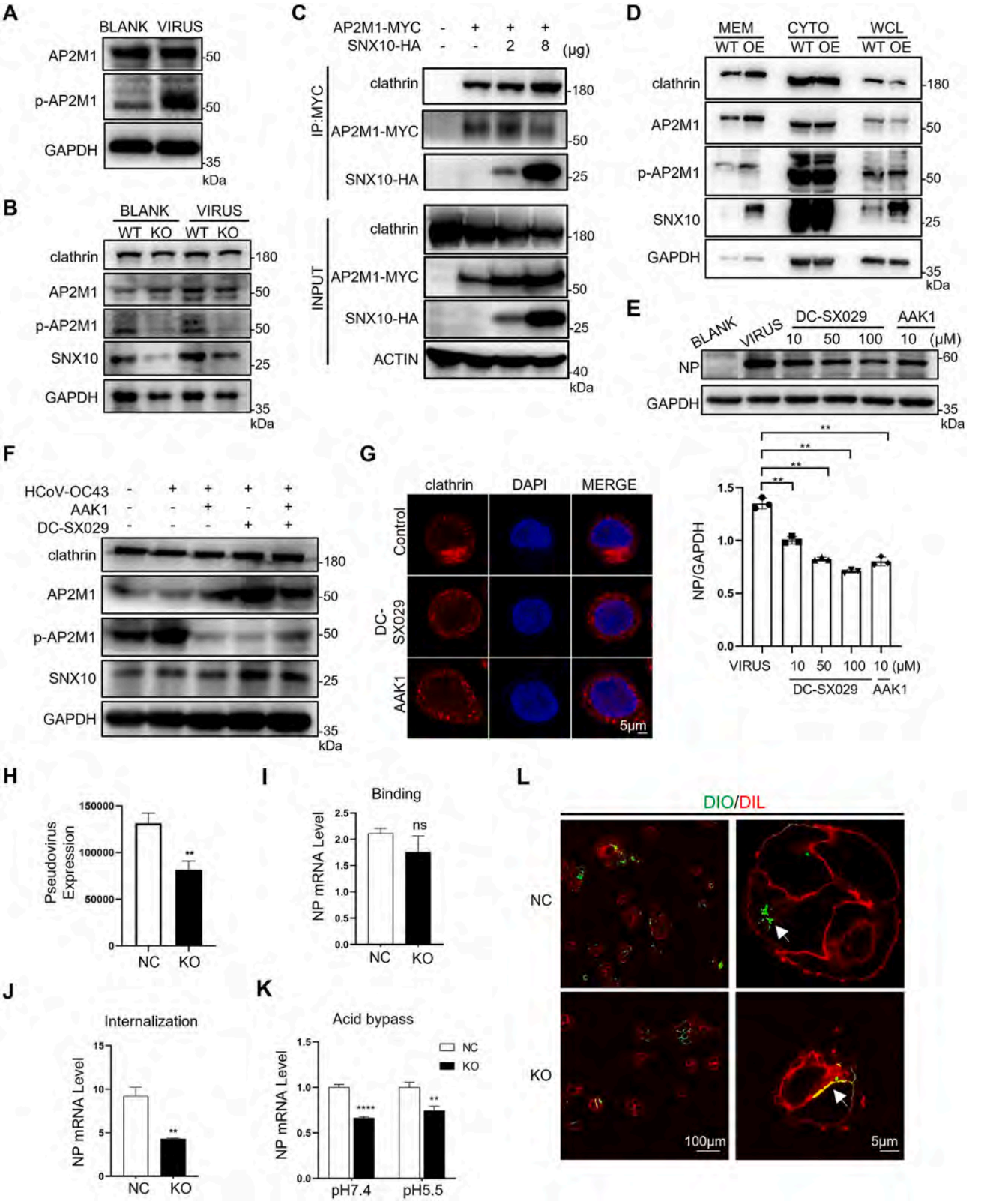

(caption on next page)

(Fig. 5A, B). Given the association of SNX10 with endosomes, we systematically assessed its impact on endosomal acidification through neutral red staining. Deletion of *SNX10* resulted in a significant reduction in acidic vacuole formation, a phenotype that was effectively restored upon SNX10 complementation (Fig. 5C). Quantitative analysis using the ratiometric pH probe Protonex™ Red 600 confirmed a reduction in acidic compartments within KO cells (Fig. 5D). Pharmacological inhibition of SNX10 resulted in a comparable attenuation of intracellular pH changes (Fig. 5E). Mechanistically, since endosomal acidification facilitates the fusion of viral envelope with endosomal membrane and subsequent genome release, our findings demonstrate that SNX10-mediated endosomal acidification serves as a critical regulator of viral genome liberation.

SNX10 deficiency activates virus-induced autophagy

Immunofluorescence co-localization analysis demonstrated that SNX10 specifically associates with early endosomes (EEA1), but shows no significant association with late endosomes (RAB7) or autolysosomes (LAMP1) (Fig. 6A). This suggests that SNX10 is selectively involved in biogenesis of endosomes. Functional assays revealed that SNX10 exhibits regulatory capacity for endosomal maturation, neither promoting the transition of early endosomes (EEs) to late endosomes (LEs) nor facilitating the conversion of LEs to autolysosomes (Fig. 6B). Lysosomal quantification using LysoSensor™ Green DND-189 demonstrated that *SNX10* knockout significantly increased lysosomal abundance (Fig. 6C, D). Adenoviral-mCherry-GFP-LC3B transduction in HCT-8 cells confirmed the enhanced formation of autolysosomes upon SNX10 depletion, which was effectively reversed through SNX10 reconstitution (Fig. 6E). Furthermore, ultrastructural analysis performed using transmission electron microscopy provided additional support for these observations (Fig. 6F).

Pharmacological inhibition employing the proteasome inhibitor MG132 (20 μM), the lysosomal inhibitor chloroquine (CQ, 50 μM), and the autophagosome-lysosome fusion inhibitor bafilomycin A1 (BAF-A1, 20 nM) demonstrated that BAF-A1 specifically modulates autophagic flux while having no effect on SNX10 protein stability (Fig. 6G). *SNX10* knockout induced characteristic autophagic markers, including an increased LC3-II/I ratio (lipidated autophagosome-associated form) and p62/SQSTM1 substrate degradation. These effects were reversed upon SNX10 reconstitution, thereby confirming the specificity of the observed phenotype (Fig. 6H). Mechanistically, the depletion of SNX10 disrupts the regulation of autophagic flux by enhancing the efficiency of autophagosome-lysosome fusion and accelerating the degradation rates of lysosomal cargo.

DISCUSSION

The emergence of three pathogenic coronaviruses (SARS-CoV, MERS-CoV, and SARS-CoV-2) in recent decades has resulted in severe human diseases, thereby highlighting the persistent threat posed by these novel coronaviruses and other emerging pathogens to global public health (Gautam et al., 2020; Harrison et al., 2020; Shang et al., 2020). Our investigation into the pathogenesis of the HCoV-OC43 virus elucidates the key mechanisms underlying coronavirus infection, thereby offering critical insights for the development of preparedness strategies against future coronavirus outbreaks.

Experimental evidence has shown that *SNX10* knockout suppresses viral replication both *in vivo* and *in vitro*. Additionally, viral infection stabilizes SNX10 protein levels, thereby underscoring its critical role in the pathogenesis of infection. We propose that HCoV-OC43 may enhance the stability of the SNX10 protein either by commandeering the E3 ubiquitin ligase (Blanchet et al., 2012) or through direct inhibition of proteasome activity (Chavoshi et al., 2016). As a host protein involved in cargo transport, SNX10 has been extensively studied for its role during the viral pre-infection phase (Amatya et al., 2021). As one of the simplest members of the SNXs family, SNX10 has been reported to play regulatory roles in the endosome pathway (Lee et al., 2022), encompassing phagocytosis and degradation of pathogens (Wang et al., 2021), antigen processing and presentation (Wu et al., 2024), inflammatory responses (You et al., 2016), and the maintenance of tissue homeostasis (Lou et al., 2017). These processes are essential for proper macrophage function. PX structural domains ensure the accurate transport of intracellular vesicles and their cargo proteins by facilitating the trafficking of specific cargo proteins from the endosome to the Golgi apparatus or the plasma membrane (Lou et al., 2021). By integrating the findings from RT-qPCR, viral envelope tracking, and immunofluorescence analysis, we propose that SNX10 facilitates viral cellular entry.

Given the critical role of SNX10 in vesicular trafficking, we first evaluated the impact of *SNX10*-knockout on viral entry. Pseudovirus assays revealed a significant inhibition of viral internalization upon *SNX10* deletion. During the early stages of infection, viral structural proteins generally interact with host membrane receptors or co-receptors to facilitate cellular entry (Boulant et al., 2015; Koehler et al., 2020). To elucidate the mechanistic involvement of SNX10, we established SNX10-overexpressing cell line and conducted immunoprecipitation-mass spectrometry (IP-MS). AP2M1 was identified as a key interacting partner. AP2M1 plays a critical role in facilitating clathrin-mediated endocytosis (CME) by promoting vesicle formation and trafficking (Ganapathy et al., 2022). The internalization of cargo *via* CME necessitates the assembly of the AP2M1-clathrin complex, which is regulated in a phosphorylation-dependent manner. Intriguingly, SNX10 knockout significantly disrupts the AP2M1 phosphorylation cycles, indicating its crucial role in CME pathways (Agajanian et al., 2019; Tongmuang et al., 2020; Wang, P.G. et al., 2020). Notably, although AP2M1-viral YxxØ motif interactions are implicated in replication enhancement (Yuan et al., 2020), this mechanism remains to be fully elucidated in our experimental system.

Our findings revealed that SNX10 directly interacts with AP2M1, the μ-subunit of the AP-2 complex, thereby enhancing AP2M1-clathrin binding during viral entry. CME is a highly conserved cellular mechanism that facilitates the internalization of extracellular cargo *via* clathrin-coated vesicles (CCVs) (Mettlen et al., 2018). Viral exploitation of CME encompasses the following sequential stages: (1) virion attachment to membrane receptors, (2) initiation of signaling cascades, (3) localized clathrin polymerization, (4) membrane invagination, and (5) CCV scission (Wang, G. et al., 2020). During this process, the recruitment of clathrin to the plasma

Fig. 4. *SNX10* deletion inhibits AP2M1 phosphorylation and suppresses viral entry into cells. **A** Western blot analysis of AP2M1 and p-AP2M1 protein expression in HCT-8 cells with HCoV-OC43 virus infection (MOI = 1) at 24 hours post-infection (hpi). **B** Western blot analysis of clathrin, AP2M1, p-AP2M1 and SNX10 protein expression in *SNX10*-knockout (KO) and control HCT-8 cells (WT) with HCoV-OC43 virus infection (MOI = 1) at 24 hpi. **C** Co-immunoprecipitation (Co-IP) for the interaction between clathrin, AP2M1 and SNX10 in 293T cells. **D** Western blot analysis of clathrin, AP2M1, p-AP2M1 and SNX10 protein expression of cell membrane, cytoplasm and whole cell lysate in SNX10-HA overexpressing (OE) and control HCT-8 cells (WT). **E** Western blot detection of viral protein NP expression after HCT-8 cell treatment with DC-SX029 (10 μM, 50 μM and 100 μM) and AAK1 (10 μM) and infected by HCoV-OC43 virus (MOI= 1) at 24 hpi. **F** Western blot analysis of clathrin, AP2M1, p-AP2M1 and SNX10 protein expression in HCT-8 cells treated with DC-SX029 or AAK1 and infected by HCoV-OC43 virus (MOI = 1) at 24 hpi. **G** Representative immunofluorescence (IF) images of clathrin expression of HCT-8 cells treated with DC-SX029 or AAK1 and infected by HCoV-OC43 virus (MOI = 10) at 2 hpi (Scale bar = 5 μm). **H** Luciferase activity assay of infection efficiency of pseudoviruses in *SNX10*-knockout (KO) and control HCT-8 (NC) cells. **I–J** RT-qPCR of viral NP mRNA level in *SNX10*-KO and control HCT-8 cells after HCoV-OC43 virus infection (MOI = 10) at binding stage (**I**), internalization stage (**J**) and acid bypass stage (**K**). **L** Representative IF images of DIO (green)/DIL (red) staining in HCT-8 cells at 2 hpi (Scale bar = 5 μm). Experiments were repeated 3 times. The data are presented as the mean ± SEM, and *P* values were calculated using two-tailed Student's *t*-test. ** $P < 0.01$.

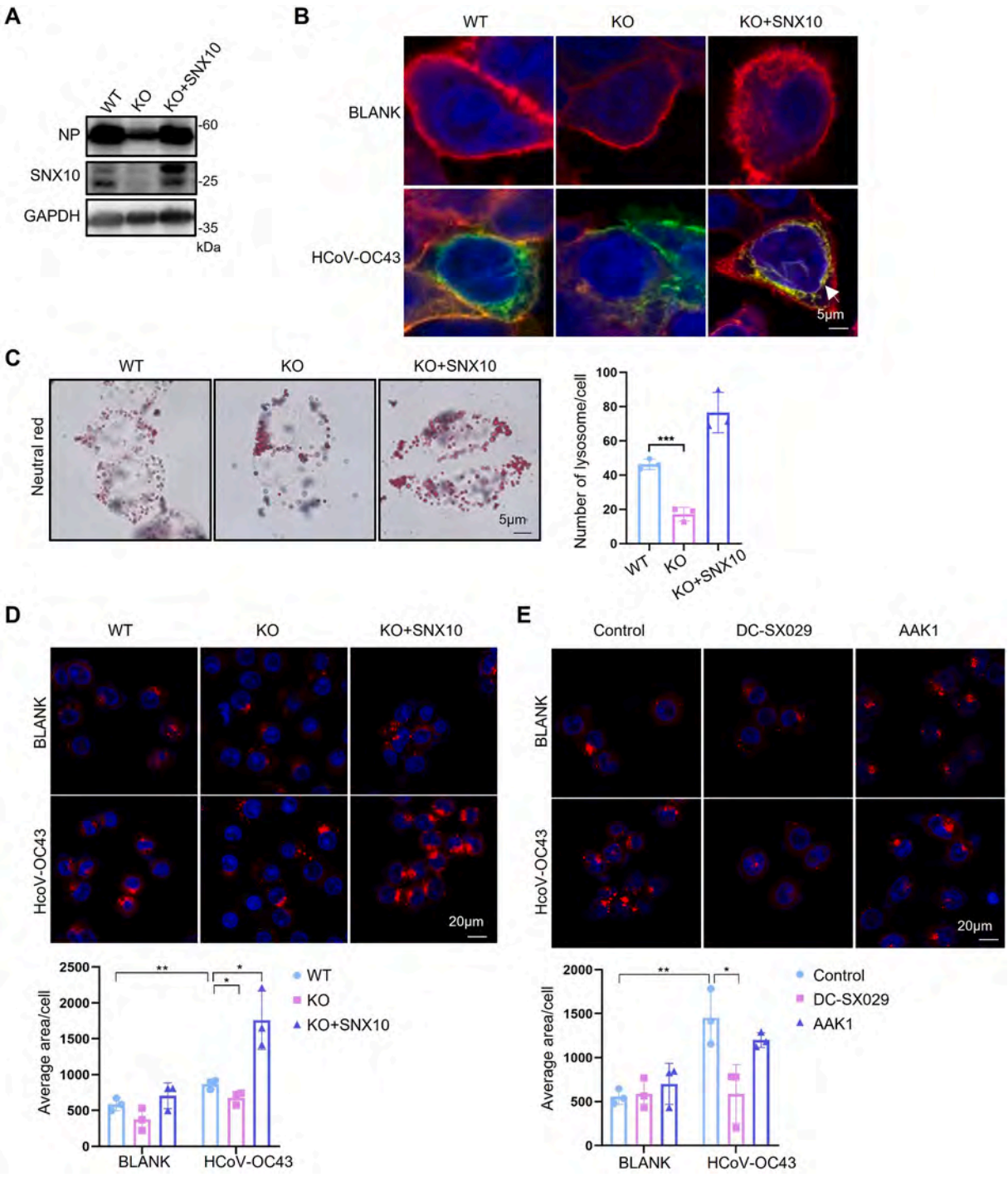

Fig. 5. SNX10 promotes cellular endosome acidification and viral release. **A** Western blot analysis of viral NP and SNX10 expression in *SNX10*-knockout (KO) and control HCT-8 (WT) cells. **B** Representative immunofluorescence (IF) images of DIO (green)/DIL (red) staining in HCT-8 cells with HCoV-OC43 infection (MOI = 10) at 2 hours post-infection (hpi) (Scale bar = 5 μm). **C** Representative images and quantification of neutral red staining to analysis the intracellular acidic vacuoles in HCT-8 cells (Scale bar = 5 μm). **D** Representative IF images and quantification of staining with pH probe Protonex™ Red 600 to analysis the change of pH in acidic endosomes of HCT-8 cells with HCoV-OC43 virus infection (MOI = 10) at 2 hpi (Scale bar = 20 μm). **E** Representative IF images and quantification of staining with pH probe Protonex™ Red 600 to analysis the change of pH in acidic endosomes of HCT-8 cells treated with DC-SX029 or AAK1 after HCoV-OC43 virus infection (MOI = 10) at 2 hpi (Scale bar = 20 μm). Experiments were repeated 3 times. The data are presented as the mean ± SEM, and p values were calculated using two-tailed Student's *t*-test. * $P < 0.05$; ** $P < 0.01$; *** $P < 0.001$.

membrane is mediated by adaptor proteins such as EPS15, AP180, AP-2 complex, and Epsin1, rather than through direct interactions with cargo receptor (Zhang et al., 2023). SNX10 plays a critical role in regulating AP2M1 phosphorylation. The inhibition of AP2M1 phosphorylation disrupts the CME complex assembly, thereby suppressing viral entry. Following cellular internalization, the release of the viral genome necessitates acidification-dependent uncoating within endosomal compartments (Fan et al., 2024). This pH-sensitive process functions as a critical molecular checkpoint for a variety of viruses, including both enveloped viruses (such as influenza viruses and coronaviruses) and non-enveloped

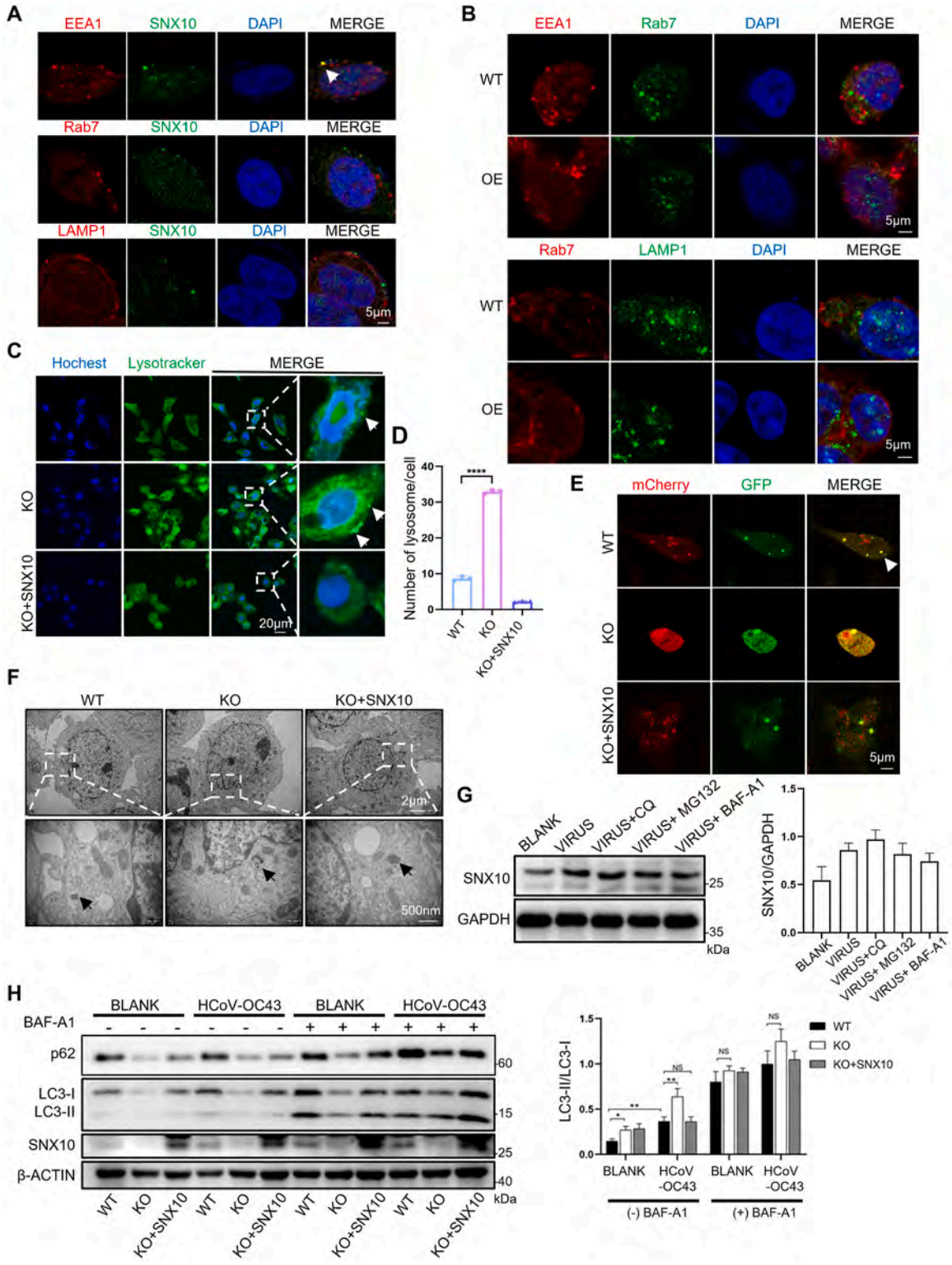

Fig. 6. SNX10 deficiency leads to activation of virus-induced autophagy. **A** Representative immunofluorescence (IF) images of the positions between SNX10 and EEA1/RAB7/LAMP1 in HCT-8 cells with HCoV-OC43 infection (MOI = 10) at 2 hours post-infection (hpi) (Scale bar = 5 μm). **B** Representative IF images of the positions between EEA1/RAB7 and RAB7/LAMP1 in SNX10-HA overexpressing (OE) and control HCT-8 cells (WT) with HCoV-OC43 infection (MOI = 10) at 2 hpi (Scale bar = 5 μm). **C, D** Representative IF images and quantification of lysosomal staining with lysosomal probe LysoTracker in *SNX10*-knockout (KO) HCT-8 cells with HCoV-OC43 virus infection (MOI = 10) at 2 hpi (Scale bar = 20 μm). **E** Representative images of staining with AdPlus-mCherry-GFP-LC3B to analysis the autophagy in HCT-8 cells with HCoV-OC43 virus infection (MOI = 10) at 2 hpi (Scale bar = 5 μm). **F** Representative images of transmission electron microscopy show the lysosomal state of HCT-8 cells with HCoV-OC43 virus infection (MOI = 10) at 2 hpi (Scale bar = 2 μm or 500 nm). **G** Western blot analysis of SNX10 protein expression in HCT-8 cells with HCoV-OC43 virus (MOI = 1) at 2 hpi, and treated with inhibitors [Chloroquine (CQ), MG132 and Bafilomycin A1 (BAF-A1)] for 4 h. **H** Western blot analysis of p62, LC3 and SNX10 protein expression in HCT-8 cells with HCoV-OC43 virus (MOI = 1) at 2 hpi, and treated with BAF-A1 for 4 h. Experiments were repeated 3 times. The data are presented as the mean ± SEM, and *P* values were calculated using two-tailed Student's *t*-test. * $P < 0.05$; ** $P < 0.01$; ns, not significant, $P > 0.05$.

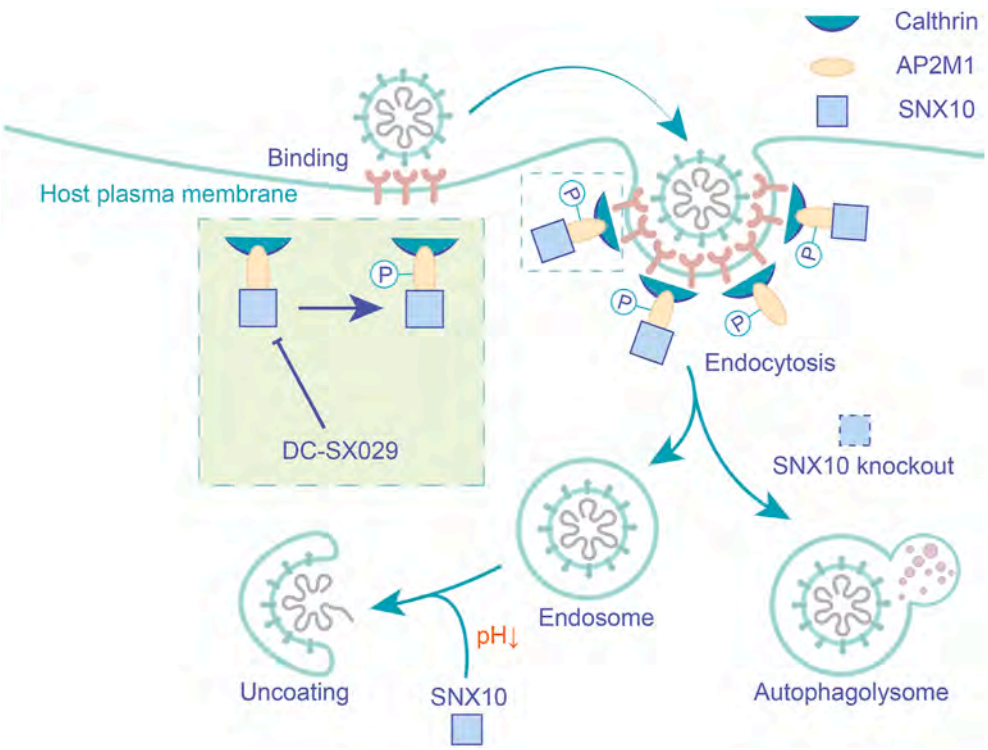

Fig. 7. The pattern diagram of SNX10 regulation of viral infection.

variants (such as rhinoviruses), to initiate infection process. Viral evolution has optimized pH-responsive structural components, such as influenza hemagglutinin and rhinovirus capsid proteins, to facilitate uncoating process (Baggen et al., 2018; Yamauchi, 2020; Müller et al., 2021). In contrast, host cells counteract viral infection by neutralizing endosomal pH or inhibiting proteases. Mechanistically, SNX10 contributes to viral genome liberation by destabilizing endosomal proton gradients *via* pH dysregulation.

It is widely recognized that cells, upon stimulation by antigens, typically activate the autophagy mechanism to eliminate these antigens and preserve the homeostasis of the intracellular environment. Likewise, when a cell is infected by a virus, it also triggers autophagy. Our studies demonstrate that SNX10-knockout during viral infection enhances early endosome biogenesis and promotes autolysosome formation *via* lysosomal conversion, indicating its crucial role in activating virus-specific autophagy pathways (Chen et al., 2023). The endosomal trafficking system consists of distinct compartments, including early endosomes, late endosomes, recycling endosomes, and lysosomes (Weeratunga et al., 2020). Notably, SNX10 promotes autophagy induced by viral infection by specifically regulating autophagosome-lysosome fusion, without influencing the maturation processes from early to late endosomes or from late endosomes to lysosomes. *SNX10* knockout induces sustained activation of autophagic flux, highlighting a complex host-pathogen interaction in which autophagy fulfills dual roles: serving as a cellular antiviral defense mechanism while also being subverted by viral strategies. While autophagy pathways eliminate invading pathogens through xenophagic degradation, evolved viral countermeasures suppress, evade, or co-opt these processes to gain a replicative advantage. Deciphering this dynamic equilibrium provides promising opportunities for the development of autophagy-modulating therapeutics.

CONCLUSIONS

In summary, this study demonstrates that SNX10 enhances coronavirus infection *via* two distinct mechanisms: (1) promoting clathrin-mediated viral entry by directly interacting with AP2M1 and (2) augmenting endosomal acidification to facilitate viral genome uncoating. Conversely, the deficiency of *SNX10* not only inhibits viral entry but also triggers autophagy in response to viral infection (Fig. 7). The dual roles of SNX10 in modulating both viral entry and autophagic processes deepen our understanding of SNX10-mediated host-virus interactions and underscore its potential as a multi-faceted target for the development of broad-spectrum antiviral therapeutics.

MATERIALS AND METHODS

Cell lines and viruses

Human return cystic cancer cells (HCT-8), human rhabdomyosarcoma cells (RD), and human embryonic kidney cells (293T) were purchased from American Type Culture Collection (ATCC, Manassas, VA, USA). 293T and RD cells were cultured in Dulbecco's modified Eagle's medium (DMEM) supplemented with 10% fetal bovine serum (FBS) and 1% penicillin/streptomycin (PS; Thermo Fisher Scientific). HCT-8 cells were maintained in RPMI1640 medium containing 1% PS and 10% FBS. HCoV-OC43 was obtained by HCT-8 cells expansion. The plaque assay was used to quantify the viral titers.

Mice

C57BL/6J mice were purchased from the Laboratory Animal Center of the Southern Medical University (Guangzhou, China). *Snx10*-flox mice were obtained from Prof. Xiaoyan Shen of the Fudan University, Shanghai, China. Genomic DNA was prepared from mouse tails using DirectPCR Lysis Reagent (Viagen Biotech) and Proteinase K (Roche). *Snx10*-flox mouse genotypes were determined by PCR using Fast PCR Master Mix (TaKaRa) and the following primer pairs: *Snx10*-F: 5'-TGTGGGAGATGATAGCTCTGATTG-3' and *Snx10*-R: 5'-TGGCCTAG AACTTACTGCAACG-3'. The PCR conditions were as follows: 94 °C 1min; 35 cycles of the amplification phase (98 °C 15s, 60 °C 30s, and 72 °C 60s), 72 °C 5min. $Snx10^{fl/fl}$ genomic DNA produced one band of 321 bp. $Snx10^{fl/-}$ genomic DNA produced two bands at 321 bp and 243 bp.

Sftpc-CreERT2 mice were purchased from Cyagen Biosciences Inc. (China). Lung epithelial cell-conditional *Snx10* knockout (*Snx10* CKO, *Snx10*$^{LEC-KO}$, *Snx10*$^{fl/fl}$; *Sftpc*-CreERT2) mice were generated by hybridizing *Snx10*-flox mice with *Sftpc*-CreERT2 mice. All mice were kept under a 12-h light/dark cycle with appropriate temperature and humidity, and had free access to food and water. All animal procedures were performed in accordance with the guidelines for the Care and Use of Laboratory Animals published by the National Institutes of Health (NIH) and were approved by the Ethics Committee of the Animal Center of Southern Medical University. Wild-type (WT) and CKO mice were intraperitoneally injected with tamoxifen (Sigma) for 5 days at 4 weeks of age, and adaptive feeding was continued for 5 days. HCoV-OC43 was infected intranasally at the end of rearing, and the mice were sacrificed 3 days later. The lung tissues were used for protein and RNA extraction to quantify viral load, as well as for histological analysis.

Antibodies and compounds

Antibodies were used for immunoblotting and immunofluorescence assay as follows: rabbit monoclonal antibody (mAb) β-actin (Cell Signaling Technology, 4970S); mouse β-actin mAb (Cell Signaling Technology, 97166); mouse polyclonal antibody (pAb) SNX10 (Santa Cruz Biotechnology, sc-293380); mouse SNX10 mAb (Novus, NBP2-45894); rabbit OC43 nucleocapsid protein (NP) mAb (Sino Biological, 40643-T62); rabbit AP2M1 mAb (ABclonal, A11070); rabbit p-AP2M1 pAb (ABclonal, AP0823); rabbit CLATHRIN mAb (Abcam, ab172958); rabbit EEA1 mAb (Abcam, ab109110); rabbit RAB7 mAb (ABclonal, A12308); mouse RAB7 mAb (Santa Cruz Biotechnology, SC-376362); rabbit LAMP1 mAb (ABclonal, A23947); rabbit P62 mAb (Proteintech, 18420-1-AP); rabbit LC3 mAb (Cell Signaling Technology, 3868); rabbit TBK1 mAb (Cell Signaling Technology, 3504); rabbit p-TBK1 mAb (Cell Signaling Technology, 5483); rabbit IRF3 mAb (Cell Signaling Technology, 4302); rabbit p-IRF3 mAb (Cell Signaling Technology, 29047); anti-HA-Tag (Cell Signaling Technology, 3724); Anti-MYC-Tag (Abmart, M20002); donkey anti-rabbit IgG (FITC) (GeneTex, GTX26798); goat anti-mouse IgG H&L (FITC) (Abcam, ab6785); HRP-conjugated goat anti-rabbit IgG (Cell Signaling Technology, 7074S); HRP-conjugated goat anti-mouse IgG (Cell Signaling Technology, 7076S); HRP-conjugated rabbit anti-goat IgG (Fdbio, FDG007). Hoechst33258 (Servicebio, G1011); DAPI (Servicebio, G1012). Cycloheximide (CHX, C7698), MG-132 (474791), Neutral Red powder (N4638), and Bafilomycin A1 (196000) were purchased from Sigma-Aldrich. Protonex™ Red 600 (Bioquest, 21207) and LysoSensor Green DND-189 (Yeasen, 40767ES50).

Cell transfection

For the overexpression assay, the expression plasmid pCMV3-mSnx10-HA or negative control pCMV3-C-HA-NCV was purchased from Sino Biological (MG51516-CY, CV013). HCT-8 cells were transfected with the plasmid pCMV3-mSnx10-HA or the negative control pCMV3-C-HA-NCV using Lipofectamine 3000 (Thermo Fisher Scientific, L3000001). To generate a stable cell line, after transduction for 24 h, the medium containing the lentivirus was replaced with RPMI1640 complete medium with 2 μg/mL puromycin. Using a single guide RNA (sgRNA), the CRISPR-Cas9 gene editing system recognizes and cleaves specific sequences, thereby knocking them out. Knockout cell line was verified using Western blotting.

Virus infection

Cells were washed twice with phosphate-buffered saline (PBS) and incubated with HCoV-OC43 (MOI = 1) (López-Muñoz et al., 2023) for 1 h. The inoculum was removed, and cells were cultured in fresh RPMI1640 blank medium, washed twice with PBS, and cultured in RPMI1640 medium supplemented with 0.1% FBS. The supernatant and protein were harvested at the indicated time points.

Plaque assay

The titer of the supernatant collected from influenza-infected cells was quantified by a plaque assay on RD cells. RD cells were washed twice and infected with serial dilutions of the samples at 37 °C for 1 h. The supernatant was discarded and replaced with 3 mL of replacement media (1.5 mL 2× DMEM and 1.5 mL Avicel supplemented with 1.5 μg/mL trypsin, 0.5% BSA, 20 mM HEPES, and 1% PS). After infection 72 h at 37 °C, cells were fixed with 4% paraformaldehyde (PFA) for 10 min at room temperature and stained with 2% crystal violet staining solution for 30 min.

Western blotting analysis

Cell lysates were prepared using RIPA lysis buffer supplemented with protease and phosphatase inhibitors. Protein samples were separated on 10% SDS-polyacrylamide gels and subsequently transferred to polyvinylidene fluoride (PVDF) membranes. After blocking with 5% non-fat milk in Tris-buffered saline (TBS) containing 0.1% Tween 20 (TBS-T) at 20–25 °C for 1 h, the protein bands were incubated with primary antibodies diluted in 5% non-fat milk at 4 °C overnight. After incubation with secondary antibodies for 1 h at 20–25 °C, the protein bands were detected using an enhanced chemiluminescent (ECL) substrate (Thermo Scientific).

RNA extraction and real-time PCR

Total RNA was extracted from tissues or cultured cells using RNA extraction kits (Foregene, RE03113, and R220701), according to the manufacturer's instructions. Rervese transscript PCR was performed using a reverse transcription kit (TaKaRa) to synthesize the first strand of cDNA from 1 mg of total RNA, using random primers. Real-time PCR was performed on a LightCycler 480II (Roche) using SYBR Green (Bio-Rad). GAPDH was used as an internal control.

Immunoprecipitation (IP) and co-immunoprecipitation (co-IP)

For immunoprecipitation and co-immunoprecipitation, cells were lysed with lysis buffer (1 M Hepes-NaOH, pH 7.6; 0.5 M EDTA; 5 M NaCl; 2.5% NP-40; and protease inhibitors), supplemented with protease inhibitors, and incubated on ice for 30 min. The cell lysates were incubated with Protein G Magnetic Beads (MCE, New Jersey, USA) and antibodies overnight at 4 °C. The beads were washed three times with lysis buffer. The bound proteins were eluted with 1 × sodium dodecyl sulfate (SDS) and analyzed by Western blotting.

Immunofluorescence assay (IF)

Immunofluorescence assays were performed as described previously. After fixation with 4% (PFA) at 20–25 °C for 20 min, the cells were permeabilized with PBS containing 0.3% Triton X-100 for 15 min. After blocking with 3% BSA for 1 h, the cells were incubated overnight with primary antibodies at 4 °C, and then secondary antibodies were added and incubated for another 1 h at 20–25 °C. The nuclei were stained with DAPI for 20 min. The samples were imaged using a confocal laser scanning microscope (LSM 880, Carl Zeiss Jena, Germany). Image processing and quantification of fluorescence signals were analyzed using Zen software.

Virus binding assay and entry assay

HCT-8 cells were inoculated into confocal dishes. After transfecting the cells with siRNA or plasmid and continued to be cultured for 2 days, the cells were infected with HCoV-OC43 (MOI = 10) (López-Muñoz

et al., 2023) in serum-free RPMI1640 and left at 4 °C for 1 h. The cells were washed three times with cold PBS, followed by the extraction of viral RNA. The cells were then washed three times with cold PBS, followed by the addition of serum-free RPMI1640 medium and placed in an incubator at 37 °C. Following incubation, the cells were treated with trypsin to remove any remaining surface-adsorbed viruses, ensuring that only the internalized viruses were retained. Finally, the cells were collected to detect the internalized viral RNA.

Acid bypass assay

HCT-8 cells were incubated once with pre-cooled blank medium and for 10 min at 4 °C. Cells were then infected with pre-cooled HCoV-OC43 viral suspension (MOI = 10) and incubated for 1 h at 4 °C to allow viral attachment to the cell surface (Dong et al., 2020). After discarding the viral inoculum, the cells were rinsed 3 times with ice-cold PBS to remove unbound viral particles. Cells were then incubated with cold PBS (pH 7.4 or pH 5.0) at 4 °C for 10 min. Afterwards, the complete medium was replaced and left at 37 °C for 2 h. Cellular RNA was collected for assay.

Membrane fluorescent staining probe DIO/DIL stain

First, the HCoV-OC43 viral suspension with DIO dye at 4 °C for 1 h, then discard the unbound dye through ultra-high speed centrifugation and re-dilution. Simultaneously, the cell membrane was stained with DIL dye. Infect the cells with the HCoV-OC43 virus bound by DIO dye at 4 °C for 1 h and washed three times with cold PBS for 3 times to wash off the unbound virus. After incubation at 37 °C incubator for 2 h, the cells were fixed with 4% PFA and observed under a microscope.

Lysosomal fluorescent probe assay

HCT-8 cells were grown to the appropriate abundance and infected with HCoV-OC43 virus (MOI = 10) on ice for 1 h, followed by a change in serum-free medium to continue incubation. The medium was aspirated, and 150 μL of probe working solution (1 μM) was added. Place in incubator at 37 °C for 1 h. Discard the supernatant and wash with PBS for 3 times, add 150 μL of Hoechst33258 working solution for 30 min, and observed through the microscope.

Acidic endosomal assay

The cells were infected with the HCoV-OC43 virus (MOI = 10) for 1 h. The cell culture medium was changed to serum-free medium after the infection and incubated in a 37 °C incubator for 1 h. The cells were washed 3 times with PBS and incubated with Protonex solution (1 μM) for 1 h at 37 °C. The supernatant was discarded, and the cells were washed with PBS for 3 times, and observed under a microscope.

Acid vacuole detection

The cells were infected with HCoV-OC43 virus (MOI = 10) for 1 h, then replaced with serum-free medium, and continued to be cultured in the 37 °C incubator. After culturing for 1 h, the cells were rinsed with PBS for 3 times. The diluted neutral red reagent was added to the cell culture dishes and incubated for 1 h at 37 °C. The supernatant was discarded, and the cells were washed with PBS for 3 times, and observed under a microscope.

Lysosomal probe staining

Cells were infected with HCoV-OC43 virus (MOI = 10) for 1 h, replaced with serum-free medium, and incubated for 2 h in an incubator. The cells were then rinsed with PBS for 3 times. The diluted LysoTracker green lysosomal probe (1 μM) was added to the dishes and incubated for 1 h. Then, the supernatant was discarded, and the cells were observed under a microscope.

Detection of cellular autophagy

Ad-mCherry-GFP-LC3B is a recombinant adenovirus that efficiently expresses the fusion proteins of the red fluorescent protein mCherry, green fluorescent protein (GFP), and LC3B in target cells after infection, with bright red and green fluorescence, which can be used for the detection of autophagy. Cells were pre-treated with Ad-mCherry-GFP-LC3B (MOI = 10) for 24 h. HCoV-OC43 virus (MOI = 10) was added to the dishes to infect the cells for 1 h, then replaced with serum-free medium and incubated for 2 h. Observations were performed under a microscope.

Pseudovirus (PsV) infection assay

Pseudoviruses were produced by the co-transfection of 293T cells with pNL4-3. Luc.R-E− and plasmids encoding either HCoV-OC43 or an empty vector using PolyJet (SignaGen). PsV supernatants were harvested at 48 h post-transfection, centrifuged at 2000×*g* for 10 min, and passed through a 0.45 μm filter to remove cell debris. For infection, HCT-8 cells were grown in 96-well plates until confluency reached 60%–80%. The respective mixtures were then added to the target cells (triplicate samples) (Romeo et al., 2020). The culture supernatants were discarded 72 h after transfection. The cells were lysed with 1 × cell lysis reagent (Promega) for 10–15 min at 20–25 °C, and the cell lysates were transferred to white opaque-walled 96-well plates. The luciferase activity was quantified using a luciferase assay kit (Promega).

Statistical analysis

An independent Student's *t*-test was performed to analyze the statistical significance between the two preselected groups. GraphPad Prism was used to generate all curves and graphs as well as for statistical analyses. Statistical significance was defined as a P -value of less than 0.05. *$P < 0.05$, ** $P < 0.01$, *** $P < 0.001$, **** $P < 0.0001$.

DATA AVAILABILITY

The mass spectrometry proteomics data have been deposited to the ProteomeXchange Consortium (https://proteomecentral.proteomexchange.org) with the dataset identifier PXD061906.

ETHICS STATEMENT

This study was performed in compliance with the institutional review board protocol of the Animal Center of Southern Medical University (SMUL202406001).

AUTHOR CONTRIBUTIONS

Haobin Li: conceptualization, data curation, formal analysis, supervision, validation, visualization, writing-original draft. Huiyi Guo: data curation, investigation. Binhao Rong: methodology, software. Haowei Li: validation, visualization. Wenjiao Wu: validation, visualization. Chan Yang: funding acquisition, supervision, writing-review & editing. Shuwen Liu: conceptualization, funding acquisition, resources, writing-review & editing.

CONFLICT OF INTEREST

The authors declare no competing interests.

ACKNOWLEDGMENTS

This work was supported by the National Natural Science Foundation (82130101), the Major Scientific and Technological Projects of Guangdong Province (2023B1111050008), and the Post Scientist Fund awarded by the Chinese Academy of Traditional Chinese Medicine (ZZ13-035-02) to Shuwen Liu. Regional Joint Foundation of Basic and Applied Basic Research in Guangdong Province (2023A1515111165) to Chan Yang.

REFERENCES

Agajanian, M.J., Walker, M.P., Axtman, A.D., Ruela-De-Sousa, R.R., Serafin, D.S., Rabinowitz, A.D., Graham, D.M., Ryan, M.B., Tamir, T., Nakamichi, Y., Gammons, M.V., Bennett, J.M., Couñago, R.M., Drewry, D.H., Elkins, J.M., Gileadi, C., Gileadi, O., Godoi, P.H., Kapadia, N., Müller, S., Santiago, A.S., Sorrell, F. J., Wells, C.I., Fedorov, O., Willson, T.M., Zuercher, W.J., Major, M.B., 2019. WNT activates the AAK1 kinase to promote clathrin-mediated endocytosis of LRP6 and establish a negative feedback loop. Cell Rep. 26, 79–93.e78.

Amatya, B., Lee, H., Asico, L.D., Konkalmatt, P., Armando, I., Felder, R.A., Jose, P.A., 2021. SNX-PXA-RGS-PXC subfamily of SNXs in the regulation of receptor-mediated signaling and membrane trafficking. Int. J. Mol. Sci. 22, 2319.

Baggen, J., Thibaut, H.J., Strating, J., Van Kuppeveld, F.J.M., 2018. The life cycle of non-polio enteroviruses and how to target it. Nat. Rev. Microbiol. 16, 368–381.

Battaglino, R.A., Jha, P., Sultana, F., Liu, W., Morse, L.R., 2019. FKBP12: a partner of Snx10 required for vesicular trafficking in osteoclasts. J. Cell. Biochem. 120, 13321–13329.

Blanchet, F.P., Mitchell, J.P., Piguet, V., 2012. β-TrCP dependency of HIV-1 Vpu-induced downregulation of CD4 and BST-2/tetherin. Curr. HIV Res. 10, 307–314.

Boulant, S., Stanifer, M., Lozach, P.Y., 2015. Dynamics of virus-receptor interactions in virus binding, signaling, and endocytosis. Viruses 7, 2794–2815.

Brian, D.A., Baric, R.S., 2005. Coronavirus genome structure and replication. Curr. Top. Microbiol. Immunol. 287, 1–30.

Chavoshi, S., Egorova, O., Lacdao, I.K., Farhadi, S., Sheng, Y., Saridakis, V., 2016. Identification of kaposi sarcoma herpesvirus (KSHV) vIRF1 protein as a novel interaction partner of human deubiquitinase USP7. J. Biol. Chem. 291, 6281–6291.

Chen, L., Yang, L., Li, Y., Liu, T., Yang, B., Liu, L., Wu, R., 2023. Autophagy and inflammation: regulatory roles in viral infections. Biomolecules 13, 1454.

Chen, Y., Liu, Q., Guo, D., 2020. Emerging coronaviruses: genome structure, replication, and pathogenesis. J. Med. Virol. 92, 418–423.

Cocucci, E., Gaudin, R., Kirchhausen, T., 2014. Dynamin recruitment and membrane scission at the neck of a clathrin-coated pit. Mol. Biol. Cell 25, 3595–3609.

Dong, X., Yang, Y., Zou, Z., Zhao, Y., Ci, B., Zhong, L., Bhave, M., Wang, L., Kuo, Y.-C., Zang, X., Zhong, R., Aguilera, E.R., Richardson, R.B., Simonetti, B., Schoggins, J.W., Pfeiffer, J.K., Yu, L., Zhang, X., Xie, Y., Schmid, S.L., Xiao, G., Gleeson, P.A., Ktistakis, N.T., Cullen, P.J., Xavier, R.J., Levine, B., 2020. Sorting nexin 5 mediates virus-induced autophagy and immunity. Nature 589, 456–461.

Fan, T., Liu, B., Yao, H., Chen, X., Yang, H., Guo, S., Wu, B., Li, X., Li, X., Xun, M., Wang, H., 2024. Cathelicidin peptide analogues inhibit EV71 infection through blocking viral entry and uncoating. PLoS Pathog. 20, e1011967.

Fehr, A.R., Perlman, S., 2015. Coronaviruses: an overview of their replication and pathogenesis. Methods Mol. Biol. 1282, 1–23.

Ganapathy, A.S., Saha, K., Suchanec, E., Singh, V., Verma, A., Yochum, G., Koltun, W., Nighot, M., Ma, T., Nighot, P., 2022. AP2M1 mediates autophagy-induced CLDN2 (claudin 2) degradation through endocytosis and interaction with LC3 and reduces intestinal epithelial tight junction permeability. Autophagy 18, 2086–2103.

Gautam, A., Kaphle, K., Shrestha, B., Phuyal, S., 2020. Susceptibility to SARS, MERS, and COVID-19 from animal health perspective. Open Vet. J. 10, 164–177.

Harrison, A.G., Lin, T., Wang, P., 2020. Mechanisms of SARS-CoV-2 transmission and pathogenesis. Trends Immunol. 41, 1100–1115.

Helbig, I., Lopez-Hernandez, T., Shor, O., Galer, P., Ganesan, S., Pendziwiat, M., Rademacher, A., Ellis, C.A., Hümpfer, N., Schwarz, N., Seiffert, S., Peeden, J., Shen, J., Štěrbová, K., Hammer, T.B., Møller, R.S., Shinde, D.N., Tang, S., Smith, L., Poduri, A., Krause, R., Benninger, F., Helbig, K.L., Haucke, V., Weber, Y.G., EuroEPINOMICS-RES Consortium; GRIN Consortium, 2019. A recurrent missense variant in AP2M1 impairs clathrin-mediated endocytosis and causes developmental and epileptic encephalopathy. Am. J. Hum. Genet. 104, 1060–1072.

Henne, W.M., Boucrot, E., Meinecke, M., Evergren, E., Vallis, Y., Mittal, R., Mcmahon, H. T., 2010. FCHo proteins are nucleators of clathrin-mediated endocytosis. Science 328, 1281–1284.

Hussain, K.M., Leong, K.L., Ng, M.M., Chu, J.J., 2011. The essential role of clathrin-mediated endocytosis in the infectious entry of human enterovirus 71. J. Biol. Chem. 286, 309–321.

Kesheh, M.M., Hosseini, P., Soltani, S., Zandi, M., 2022. An overview on the seven pathogenic human coronaviruses. Rev. Med. Virol. 32, e2282.

Koehler, M., Delguste, M., Sieben, C., Gillet, L., Alsteens, D., 2020. Initial step of virus entry: virion binding to cell-surface glycans. Annu. Rev. Virol. 7, 143–165.

Kong, N., Shan, T., Wang, H., Jiao, Y., Zuo, Y., Li, L., Tong, W., Yu, L., Jiang, Y., Zhou, Y., Li, G., Gao, F., Yu, H., Zheng, H., Tong, G., 2020. BST2 suppresses porcine epidemic diarrhea virus replication by targeting and degrading virus nucleocapsid protein with selective autophagy. Autophagy 16, 1737–1752.

Lee, W., Kim, H.Y., Choi, Y.J., Jung, S.H., Nam, Y.A., Zhang, Y., Yun, S.H., Chang, T.S., Lee, B.H., 2022. SNX10-mediated degradation of LAMP2A by NSAIDs inhibits chaperone-mediated autophagy and induces hepatic lipid accumulation. Theranostics 12, 2351–2369.

Liao, Z., Si, T., Kai, J.J., Fan, J., 2024. Mechanism of membrane curvature induced by SNX1: insights from molecular dynamics simulations. J. Phys. Chem. B 128, 2144–2153.

Liu, Q., Bautista-Gomez, J., Higgins, D.A., Yu, J., Xiong, Y., 2021. Dysregulation of the AP2M1 phosphorylation cycle by LRRK2 impairs endocytosis and leads to dopaminergic neurodegeneration. Sci. Signal. 14, eabg3555.

López-Muñoz, A.D., Santos, J.J.S., Yewdell, J.W., 2023. Cell surface nucleocapsid protein expression: a Betacoronavirus immunomodulatory strategy. Proc Natl Acad Sci U S A 120, e2304087120.

Lou, J., Li, X., Huang, W., Liang, J., Zheng, M., Xu, T., Lyu, J., Li, D., Xu, Q., Jin, X., Fu, G., Wang, D., Lu, L., 2017. SNX10 promotes phagosome maturation in macrophages and protects mice against Listeria monocytogenes infection. Oncotarget 8, 53935–53947.

Lou, Y., Zhang, J., Wang, G., Fang, W., Wang, S., Abubakar, Y.S., Zhou, J., Wang, Z., Zheng, W., 2021. Genome-wide characterization of PX domain-containing proteins involved in membrane trafficking-dependent growth and pathogenicity of Fusarium graminearum. mBio 12, e0232421.

Lu, Y., He, P., Zhang, Y., Ren, Y., Zhang, L., 2022. The emerging roles of retromer and sorting nexins in the life cycle of viruses. Virol. Sin. 37, 321–330.

Malik, Y.A., 2020. Properties of coronavirus and SARS-CoV-2. Malays. J. Pathol. 42, 3–11.

Malone, B., Urakova, N., Snijder, E.J., Campbell, E.A., 2022. Structures and functions of coronavirus replication-transcription complexes and their relevance for SARS-CoV-2 drug design. Nat. Rev. Mol. Cell Biol. 23, 21–39.

Mettlen, M., Chen, P.H., Srinivasan, S., Danuser, G., Schmid, S.L., 2018. Regulation of clathrin-mediated endocytosis. Annu. Rev. Biochem. 87, 871–896.

Miller, K., Mcgrath, M.E., Hu, Z., Ariannejad, S., Weston, S., Frieman, M., Jackson, W.T., 2020. Coronavirus interactions with the cellular autophagy machinery. Autophagy 16, 2131–2139.

Müller, T.G., Zila, V., Peters, K., Schifferdecker, S., Stanic, M., Lucic, B., Laketa, V., Lusic, M., Müller, B., Kräusslich, H.G., 2021. HIV-1 uncoating by release of viral cDNA from capsid-like structures in the nucleus of infected cells. eLife 10, e64776.

Norris, A., Tammineni, P., Wang, S., Gerdes, J., Murr, A., Kwan, K.Y., Cai, Q., Grant, B.D., 2017. SNX-1 and RME-8 oppose the assembly of HGRS-1/ESCRT-0 degradative microdomains on endosomes. Proc. Natl. Acad. Sci. U. S. A. 114, E307–E316.

Peng, Y., Du, N., Lei, Y., Dorje, S., Qi, J., Luo, T., Gao, G.F., Song, H., 2020. Structures of the SARS-CoV-2 nucleocapsid and their perspectives for drug design. EMBO J. 39, e105938.

Schmidt, O., Weyer, Y., Fink, M.J., Müller, M., Weys, S., Bindreither, M., Teis, D., 2017. Regulation of Rab5 isoforms by transcriptional and post-transcriptional mechanisms in yeast. FEBS Lett. 591, 2803–2815.

Shang, J., Wan, Y., Luo, C., Ye, G., Geng, Q., Auerbach, A., Li, F., 2020. Cell entry mechanisms of SARS-CoV-2. Proc. Natl. Acad. Sci. U. S. A. 117, 11727–11734.

Tan, Y.J., Lim, S.G., Hong, W., 2006. Understanding the accessory viral proteins unique to the severe acute respiratory syndrome (SARS) coronavirus. Antivir. Res. 72, 78–88.

Tian, Y., Kang, Q., Shi, X., Wang, Y., Zhang, N., Ye, H., Xu, Q., Xu, T., Zhang, R., 2021. SNX-3 mediates retromer-independent tubular endosomal recycling by opposing EEA-1-facilitated trafficking. PLoS Genet. 17, e1009607.

Tongmuang, N., Yasamut, U., Noisakran, S., Sreekanth, G.P., Yenchitsomanus, P.T., Limjindaporn, T., 2020. Suppression of μ1 subunit of the adaptor protein complex 2 reduces dengue virus release. Virus Genes 56, 27–36.

Tscherne, D.M., Jones, C.T., Evans, M.J., Lindenbach, B.D., Mckeating, J.A., Rice, C.M., 2006. Time- and temperature-dependent activation of hepatitis C virus for low-pH-triggered entry. J. Virol. 80, 1734–1741.

Van Weering, J.R., Verkade, P., Cullen, P.J., 2010. SNX-BAR proteins in phosphoinositide-mediated, tubular-based endosomal sorting. Semin. Cell Dev. Biol. 21, 371–380.

Vijgen, L., Keyaerts, E., Moës, E., Thoelen, I., Wollants, E., Lemey, P., Vandamme, A.M., Van Ranst, M., 2005. Complete genomic sequence of human coronavirus OC43: molecular clock analysis suggests a relatively recent zoonotic coronavirus transmission event. J. Virol. 79, 1595–1604.

Wang, C., Hesketh, E.L., Shamorkina, T.M., Li, W., Franken, P.J., Drabek, D., Van Haperen, R., Townend, S., Van Kuppeveld, F.J.M., Grosveld, F., Ranson, N.A., Snijder, J., De Groot, R.J., Hurdiss, D.L., Bosch, B.J., 2022. Antigenic structure of the human coronavirus OC43 spike reveals exposed and occluded neutralizing epitopes. Nat. Commun. 13, 2921.

Wang, G., Jiang, L., Wang, J., Zhang, J., Kong, F., Li, Q., Yan, Y., Huang, S., Zhao, Y., Liang, L., Li, J., Sun, N., Hu, Y., Shi, W., Deng, G., Chen, P., Liu, L., Zeng, X., Tian, G., Bu, Z., Chen, H., Li, C., 2020a. The G protein-coupled receptor FFAR2 promotes internalization during influenza A virus entry. J. Virol. 94, e01707–e01719.

Wang, P.G., Tang, D.J., Hua, Z., Wang, Z., An, J., 2020b. Sunitinib reduces the infection of SARS-CoV, MERS-CoV and SARS-CoV-2 partially by inhibiting AP2M1 phosphorylation. Cell Discov 6, 71.
Wang, X., Ni, J., You, Y., Feng, G., Zhang, S., Bao, W., Hou, H., Li, H., Liu, L., Zheng, M., Wang, Y., Zhou, H., Shen, W., Shen, X., 2021. SNX10-mediated LPS sensing causes intestinal barrier dysfunction via a caspase-5-dependent signaling cascade. EMBO J. 40, e108080.
Weeratunga, S., Paul, B., Collins, B.M., 2020. Recognising the signals for endosomal trafficking. Curr. Opin. Cell Biol. 65, 17–27.
Wu, D., Wang, Y., Xu, J., Wang, D., Zhang, J., Meng, L., Hu, Y., Wang, P., Lin, J., Zhou, S., 2024. SNX10 promoted liver IR injury by facilitating macrophage M1 polarization via NLRP3 inflammasome activation. Mol. Immunol. 166, 79–86.
Yamauchi, Y., 2020. Influenza A virus uncoating. Adv. Virus Res. 106, 1–38.
You, Y., Li, W.Z., Zhang, S., Hu, B., Li, Y.X., Li, H.D., Tang, H.H., Li, Q.W., Guan, Y.Y., Liu, L.X., Bao, W.L., Shen, X., 2018. SNX10 mediates alcohol-induced liver injury and steatosis by regulating the activation of chaperone-mediated autophagy. J. Hepatol. 69, 129–141.
You, Y., Zhou, C., Li, D., Cao, Z.L., Shen, W., Li, W.Z., Zhang, S., Hu, B., Shen, X., 2016. Sorting nexin 10 acting as a novel regulator of macrophage polarization mediates inflammatory response in experimental mouse colitis. Sci. Rep. 6, 20630.
Yousefi, M., Lee, W.S., Yan, B., Cui, L., Yong, C.L., Yap, X., Tay, K.S.L., Qiao, W., Tan, D., Nurazmi, N.I., Linster, M., Smith, G.J.D., Lee, Y.H., Carette, J.E., Ooi, E.E., Chan, K.R., Ooi, Y.S., 2022. TMEM41B and VMP1 modulate cellular lipid and energy metabolism for facilitating dengue virus infection. PLoS Pathog. 18, e1010763.
Yuan, S., Chu, H., Huang, J., Zhao, X., Ye, Z.W., Lai, P.M., Wen, L., Cai, J.P., Mo, Y., Cao, J., Liang, R., Poon, V.K., Sze, K.H., Zhou, J., To, K.K., Chen, Z., Chen, H., Jin, D. Y., Chan, J.F., Yuen, K.Y., 2020. Viruses harness YxxØ motif to interact with host AP2M1 for replication: a vulnerable broad-spectrum antiviral target. Sci. Adv. 6, eaba7910.
Zhang, Y., Srivastava, V., Zhang, B., 2023. Mammalian cargo receptors for endoplasmic reticulum-to-Golgi transport: mechanisms and interactions. Biochem. Soc. Trans. 51, 971–981.